

# Low-Order Bessel-Type PID Dynamics in Lithium-Based Tritium Breeding and Heat-Removal Systems

S. A. S. Borges and S. D. Campos\*

*Applied Mathematics Laboratory, DFQM/CCTS,*

*Federal University of São Carlos, CEP 18052-780, Sorocaba, SP, Brazil*

Lithium plays a dual role in deuterium–tritium fusion systems by enabling tritium breeding in blankets and providing an efficient heat-removal medium in liquid-metal components. Here, we combine nuclear data for deuterium–tritium and lithium reactions with a reduced thermohydraulic model of a liquid lithium jet and an operator-theoretic formulation of feedback control. We derive a low-order model for jet thermal expansion under deuteron-beam loading and show that a continuous-time proportional–integral–derivative controller, written in operator form, can be locally embedded in a family of Bessel-type differential operators acting on the tritium-inventory error. The results suggest that lithium-based breeding and heat-removal systems admit low-order, proportional–integral–derivative controllable dynamics that can be interpreted in terms of localized Bessel modes, providing a compact analytical framework for guiding future controller design and blanket/jet optimization.

## I. INTRODUCTION

The climate crisis and the need to decarbonize the global energy mix motivate the search for energy sources with low greenhouse gas emissions and reduced production of long-lived hazardous waste [1, 2]. Among the options under study, controlled nuclear fusion based on deuterium–tritium (D–T) reactions is widely seen as a promising path to large-scale, low-carbon power, offering high power density, limited long-lived radioactive waste, and a low risk of catastrophic accidents compared with conventional fission [1–4].

In magnetically confined plasmas, such as those produced in tokamak devices, a toroidal vacuum vessel surrounded by electromagnetic coils that create a strong helical magnetic field to confine and heat the plasma [5–8]. In this configuration, the D-T reaction combines the largest fusion cross section at comparatively low ion temperatures with a favorable energy balance, making it the leading candidate for near-term fusion power plants [3, 4, 9, 10]. Achieving tritium self-sufficiency in these systems requires the integration of tritium-breeding blankets, in which lithium (Li) plays a dual

---

\* sergiode@ufscar.br

role: it acts as a breeding material via neutron-induced reactions on  ${}^6\text{Li}$  and  ${}^7\text{Li}$ , simultaneously serving as a medium for heat removal in liquid-metal blankets and high-speed Li jets [11–18].

Recent design advancements in large-scale magnetic confinement fusion programs underscore the increasingly stringent performance and reliability requirements placed on first-wall and blanket structural and functional materials. Notably, the revised ITER baseline configuration has replaced beryllium with tungsten as the first-wall material. This modification raises the kinetic energy threshold for deuterium-induced surface damage and erosion, substantially suppresses physical sputtering, and correspondingly tightens the design and operational constraints on plasma-facing and blanket components with respect to plasma compatibility, thermal load management, and neutron-induced damage and activation control [19, 20]. Analogous design considerations are encountered in EU DEMO investigations, wherein multiple blanket concepts—in particular the Helium-Cooled Lithium Lead (HCLL), Helium-Cooled Pebble Bed (HCPB), and water-cooled lead–ceramic configurations (WCLL/WLCB)—systematically examine distinct combinations of liquid PbLi breeding materials, neutron multipliers, and advanced ceramic breeder systems [21–25]. In all these designs, Li-based components are central to closing the D-T fuel cycle and managing the high heat loads associated with fusion plasmas [11–16].

From a neutronics perspective, a principal performance metric for D–T fusion reactors is the tritium breeding ratio (TBR), defined as the ratio between the time-dependent tritium production rate in the breeding blanket and the tritium consumption rate as fusion fuel [11–13, 25–27]. While tritium self-sufficiency requires at minimum  $\text{TBR} \geq 1$ , practical considerations, including inventory losses, processing delays, and the need for safety and operational margins, necessitate operating regimes in which TBR exceeds unity by a non-negligible amount [11–13, 26, 27]. Comprehensive Monte Carlo neutronics and burnup analyzes demonstrate that TBR exhibits a nonlinear dependence on blanket geometry, material composition, and neutron energy spectra, and that securing sufficient breeding margins within realistic blanket configurations constitutes a stringent and non-trivial constraint on overall reactor feasibility [11–13, 24–28].

In parallel, lithium also appears in high-intensity neutron-source concepts based on deuteron beams incident on high-speed liquid Li jets, such as the International Fusion Materials Irradiation Facility - DEMO Oriented NEutron Source (IFMIF-DONES) [29–32]. In these facilities, the D-Li stripping reaction is used to generate neutron spectra similar to those from D-T fusion, exposing test materials to fusion-relevant conditions [29–32]. The free-surface Li jet in IFMIF-type systems must withstand substantial energy and momentum deposition from the deuteron beam, which drives strong thermal gradients, surface perturbations, and flow instabilities that place additional design

and operating constraints on the target and associated heat-removal systems [17, 29–32].

Because both tokamak blankets and Li-jet targets must operate near design points with small, controlled deviations in TBR, temperature, and flow parameters, feedback control strategies are essential to keep key observables within acceptable bounds [16, 24, 25, 33, 34]. Previous work on tritium breeding control within liquid-metal blankets has shown that relatively simple proportional–integral–derivative (PID) controllers can regulate the  ${}^6\text{Li}:{}^7\text{Li}$  enrichment ratio and maintain TBR near a target value, based on local linearizations of more complex neutronics models [16, 24, 25, 34]. However, most of the existing literature treats neutronics, thermohydraulics, and feedback control as largely separate layers. There is currently no compact analytical framework that connects Li-based tritium breeding, jet thermohydraulics, and PID control in a way that illuminates the underlying dynamical structure and can guide controller tuning and system design [16, 24, 25, 33, 34].

In this work, we address this gap by combining nuclear data for D-T and Li reactions with a reduced-order thermohydraulic model of a liquid Li jet, complemented by an operator-theoretic formulation of the feedback control system. First, we review the basic physics of D-T fusion and the principal Li-based nuclear reactions responsible for tritium production, emphasizing their impact on TBR and blanket performance [9–15, 26–28, 35, 36]. Second, we formulate a reduced-order thermohydraulic model for jet thermal expansion based on coupled mass and heat transport equations that govern the response of a liquid Li jet to energy and momentum deposition from a deuteron beam [17, 18, 29–32]. Third, we introduce the continuous-time PID controller in operator form and show that, after localization around a reference operating point, it is locally equivalent to a Bessel-type differential operator acting on the tritium-inventory error [33, 34, 37]. By constructing a simple second-order error-dynamics model, we derive an explicit correspondence between the PID gains and effective Bessel parameters and illustrate this mapping with numerical examples [33, 34, 37].

Our results indicate that Li-based breeding and heat-removal systems exhibit low-order. These PID-controllable dynamics can be interpreted in terms of localized Bessel modes, providing a unified perspective on tritium breeding, thermal management, and feedback control in Li-based fusion technologies [16, 24, 25, 29, 30, 33, 34, 37].

The paper is organized as follows. Section II reviews the basic physics of D-T fusion and the main Li-based T-breeding reactions. Section III presents the reduced description of jet thermal expansion under deuteron-beam loading. Section IV introduces the PID operator and the Bessel differential recurrences and develops the PID–Bessel correspondence. Section V connects this framework to

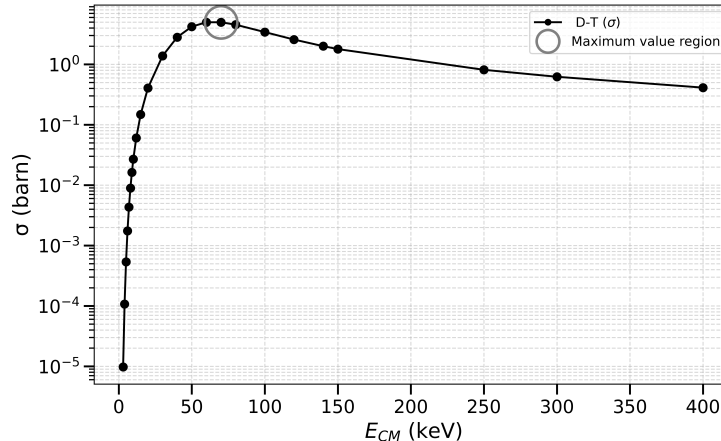
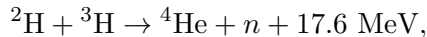


Figure 1. Total cross section for D–T collisions as a function of the center-of-mass energy  $E_{CM}$ . The red circle marks the maximum  $\sigma \approx 5.0$  barns at  $E_{CM} \approx 65$  keV, a range compatible with ion temperatures envisaged for near-term D–T reactors. Experimental data are from Ref. [9].

the tritium breeding ratio. Section VI illustrates the ideas with a reduced jet/blanket–PID model, and Section VII summarizes our conclusions and discusses prospects for future work.

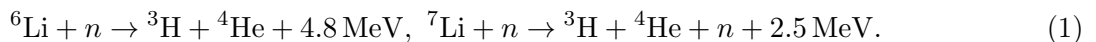
## II. D-T FUSION

The most relevant fusion reaction for energy applications is D-T fusion,



which combines a large cross-section at relatively low energies with a favorable energy balance, making it the natural candidate for the first commercial fusion reactors. Figure 1 shows the total cross section,  $\sigma$  (barn), for several center-of-mass energies,  $E_{CM}$  (keV), for D-T collisions. The maximum value of  $\sigma_{max}$  ( $\approx 5.0$  barns) is achieved at relatively low energies ( $\approx 65$  keV). The combination of the great value for the  $\sigma$  at low energies is especially interesting when compared to the D- ${}^3\text{He}$ , where  $\sigma_{max} \approx 0.8$  barn at  $E_{CM} \approx 600$  keV [36].

However, tritium is practically absent in nature because it is radioactive and has a relatively short half-life of 12.32 years [28]. Tritium can be generated by the interaction of neutrons and lithium, produced *in situ*, typically from reactions involving lithium in breeding blankets through two main reactions



At the same time, 14.1 MeV neutrons carry most of the released energy and must be properly absorbed and converted into useful heat. In this context, lithium plays a promising dual role: on the one hand, it acts as a tritium breeding material via reactions with neutrons [16], and on the other hand, it can serve as a medium for heat containment and transport in the form of liquid metal in contact with the neutron flux and, in some concepts, with the plasma itself [17, 18, 38]. Moreover, concepts of intense neutron sources based on high-energy deuteron beams incident on high-speed liquid lithium jets have been proposed and studied as material test facilities for fusion reactors, exploiting the D–Li stripping reaction to generate neutrons with spectra similar to those from the D–T reaction [31, 32].

One of the key performance parameters for deuterium–tritium fusion reactors is the tritium breeding ratio (TBR). It is defined as the ratio between the time-dependent rate of tritium production within the breeding blanket,  $TP(t)$ , of the reactor and the time-dependent rate at which tritium is consumed,  $TC(t)$ , as fuel in the fusion reactions. Therefore, one writes

$$\text{TBR}(t) = \frac{TP(t)}{TC(t)}. \quad (2)$$

For self-sufficiency, the minimum required is  $\text{TBR} = 1$ . However, tritium losses are expected, and a more realistic estimate should account for uncertainties and/or deficiencies [13, 26, 27]. Then, a 10% safety margin can be used to account for uncertainties [11, 12]. Considering reactions (1), TBR is nonlinear. It can be increased by optimizing the  ${}^6\text{Li}$  and  ${}^7\text{Li}$  atomic fractions for the neutron energy spectrum, and by increasing both the neutron flux and the breeding blanket volume.

### III. JET THERMAL EXPANSION

We here develop a reduced description of the thermal expansion of a liquid Li jet subjected to intense deuteron-beam loading to obtain low-order observables that can later be used in feedback-control models [29, 30]. The emphasis is not on reproducing the full three-dimensional computational fluid dynamics behavior of IFMIF-type targets, but rather on capturing the dominant thermohydraulic couplings in a form suitable for subsequent linearization and control design [29, 30].

Figure 2 depicts the D beam colliding with the Li transverse jet in facilities such as the International Fusion Materials Irradiation Facility – DEMO Oriented Neutron Source (IFMIF-DONES) [29, 30]. The target system employs a free-surface liquid Li-jet about 25 mm thick and 260 mm wide, flowing at velocities of the order of 15 m/s in front of the deuteron beam, with an average surface heat flux of several  $10^8$  W/m<sup>2</sup> corresponding to a total deposited power of  $\sim 5$  MW.

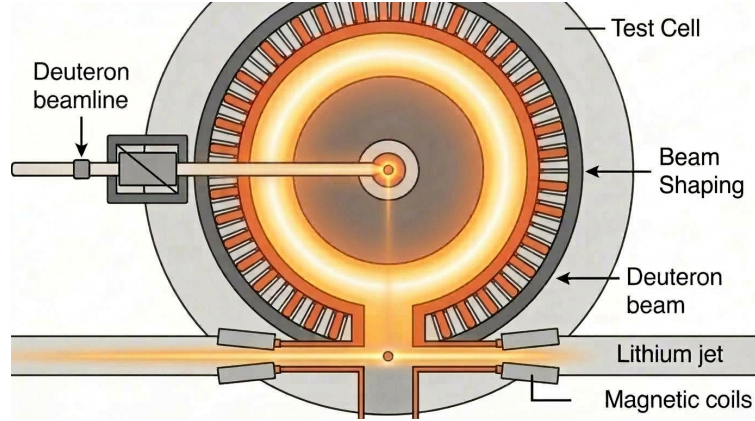


Figure 2. Schematic interaction between a deuteron beam and a free-surface liquid Li jet in IFMIF-DONES-type facilities. The configuration reproduces fusion-relevant neutron irradiation conditions for test materials while imposing stringent constraints on jet stability, heat removal, and surface integrity.

In current EU DEMO studies, the main blanket concepts are: the Helium Cooled Lithium Lead (HCLL) blanket, using liquid PbLi as breeder and neutron multiplier; the Helium Cooled Pebble Bed (HCPB) blanket, using ceramic breeder pebble beds of lithiated compounds such as  $\text{Li}_4\text{SiO}_4$  and  $\text{Li}_2\text{TiO}_3$ ; and water-cooled lead-ceramic variants (WCLL/WLCB), which combine Pb or PbLi multipliers with advanced ceramic breeders in tube or pebble bed configurations [21–23].

In tokamak devices, by contrast, Li is not introduced predominantly as an energetic beam impinging on metallic targets but rather as a constituent of the gaseous fuel mixture that is ionized to form the fusion plasma (together with tritium). Li is incorporated into the vessel structures, specifically within the breeding blanket that surrounds the plasma. Its principal functions in this configuration are (i) to capture the high-energy neutrons produced by the D-T fusion reactions to breed T *in situ*, and (ii) to participate in thermal management by facilitating the removal of heat, which can then be converted into electrical power.

To model the coupling between the velocity field and the thermal expansion of the jet, we start from the mass-conservation equation, written as

$$\frac{\partial \rho}{\partial t} + \nabla \cdot (\rho \vec{v}) = 0 \quad (3)$$

where  $\rho = \rho(x, y, z, t)$  is the mass density and  $\vec{v} = (v_x, v_y, v_z)$  is the velocity distribution inside the flowing jet [17, 18, 30]. For the reduced model considered here, we assume that the jet is weakly compressible over the operating range of interest, so that density variations are small but not strictly zero and can be driven by temperature changes and beam-induced perturbations [17, 18, 30]. In

addition, we adopt a simple parametrization for the transverse components of the velocity,

$$v_x = k_x v, \quad v_y = k_y v, \quad (4)$$

where  $v$  is a characteristic jet-flow velocity and  $k_x, k_y$  are dimensionless parameters that encode the relative magnitude of the transverse components. Substituting equation (4) into equation (3) and collecting terms, we obtain an equation for the longitudinal component  $v_z$  of the velocity,

$$\frac{\partial \rho}{\partial t} + k_x v_x \frac{\partial \rho}{\partial x} + k_y v_y \frac{\partial \rho}{\partial y} + \frac{\partial}{\partial z} (\rho v_z) = 0, \quad (5)$$

interpreted as governing the maximum perturbation velocity in the  $z$ -direction along the jet [17, 18, 30].

The evolution of the temperature field is described by the time-dependent heat-conduction equation with advection,

$$\rho C_p \left( \frac{\partial T}{\partial t} + \vec{v} \cdot \nabla T \right) - \nabla \cdot (\lambda \nabla T) = q(x, y, z, t), \quad (6)$$

where  $T = T(x, y, z, t)$  is the temperature,  $C_p$  is the specific heat capacity,  $\lambda$  is the thermal conductivity of Li, and  $q$  is the volumetric heat source associated with energy deposition from the deuteron beam [17, 18, 30]. In the IFMIF-DONES geometry, the jet can be approximated as a planar slab with thickness  $h$  along one transverse direction and width  $w$  in the orthogonal transverse direction, with the beam primarily depositing energy over a finite interaction length in  $z$  [29, 30]. For the reduced-order representation, equation (6) may be averaged over the thickness  $h$  and/or the width  $w$ , thereby yielding an effective one-dimensional or quasi-two-dimensional formulation for  $T(z, t)$  or  $T(y, z, t)$ , respectively. This procedure retains the leading-order interactions among beam loading, advective transport, and thermal conduction [17, 18, 30].

Figure 3 illustrates representative solutions of the coupled system formed by equation (5) and (6) for a set of parameters characteristic of IFMIF-type operation. In particular, the figure presents the maximum longitudinal perturbation velocity  $v_z$  (in logarithmic scale) toward the front surface as a function of the beam and flow parameters, thereby demonstrating that intense energy deposition gives rise to localized perturbations of velocity and temperature that remain confined within the beam-matter interaction region [17, 29, 30]. These perturbations introduce stringent constraints on the admissible operating regimes, including, for example, upper bounds on allowable surface temperature increases and on the maximum velocity deviation with respect to the mean flow [17, 29, 30].

The foregoing analysis demonstrates that the full fields  $\rho(x, y, z, t)$  and  $T(x, y, z, t)$ , governed by equations (5) and (6), can be systematically reduced to a low-dimensional set of scalar observables

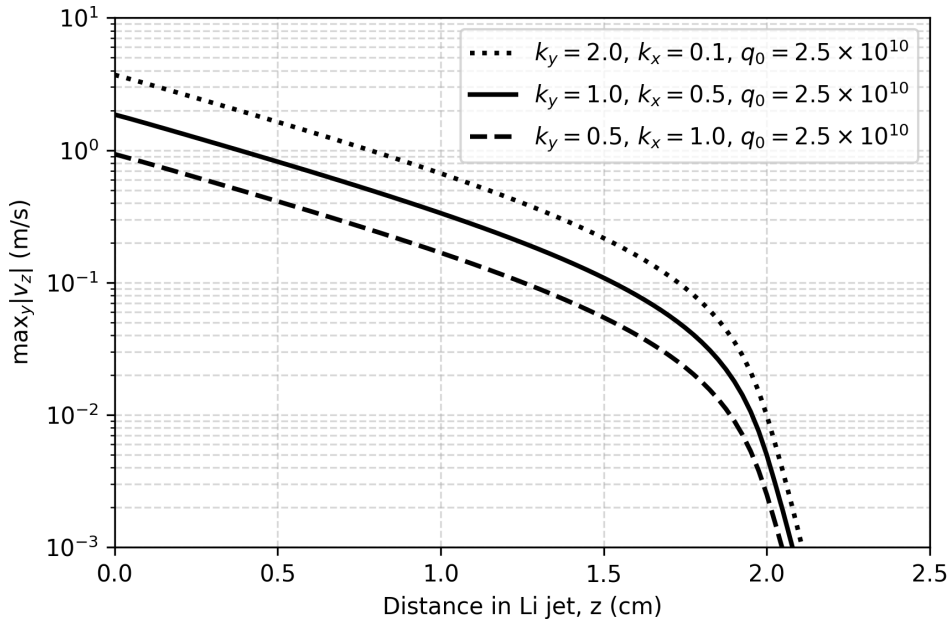


Figure 3. Different values for the maximum velocity  $v_z$  (in logarithmic scale) toward the front surface.

that are more directly pertinent to feedback-control design [17, 24, 29, 30]. Examples include the maximum jet temperature at the front surface,  $T_{\max}(t)$ ; the peak transverse or longitudinal velocity perturbation,  $v_{z,\max}(t)$ ; and integrated figures of merit that jointly characterize tritium-production efficiency and heat-removal performance [16, 24, 25, 29, 30]. Upon linearization of equations (5) and (6) about a steady operating point of the jet/blanket system and subsequent projection onto these observables, the resulting dynamics can be represented with high fidelity by low-order, linear time-invariant models over the relevant operating regime [16, 24, 25].

Schematically, one can summarize this reduction chain as

$$(\rho(x, y, z, t), T(x, y, z, t)) \rightarrow \{y_i(t)\} \rightarrow \text{low-order LTI model} \rightarrow \text{PID/Bessel operator design},$$

where  $\{y_i(t)\}$  denotes a small set of scalar observables extracted from the full fields [16, 24, 25, 34]. In the next section, we demonstrate that the standard PID controller, expressed in operator form, together with the differential recurrence relations for Bessel functions, furnishes a convenient abstract framework for characterizing the feedback shaping of low-order error dynamics. Within this framework, PID-based tritium and thermal control schemes can be understood as specific instances of a more general Bessel-type operator structure.

#### IV. PID OPERATOR AND BESSEL DIFFERENTIAL RECURRENCES

We recast the standard continuous-time PID law here in operator form and compare it with the differential recurrences of Bessel functions, thereby identifying a local correspondence between PID-based error dynamics and a family of Bessel-type operators.

The continuous-time PID controller can be written as [33, 34]

$$u(t) = K \left( e(t) + \frac{1}{T_i} \int_0^t e(\tau) d\tau + T_d \frac{de}{dt}(t) \right), \quad (7)$$

where  $e(t)$  is the error signal,  $K$  is the proportional gain, and  $T_i$  and  $T_d$  are the integral and derivative time constants, respectively. The mathematical structure of the PID equation (7) can be viewed as the action of a linear operator  $C$  on  $e$

$$u(t) = C[e](t),$$

with

$$C := K \left( I + \frac{1}{T_i} \mathcal{I} + T_d \mathcal{D} \right), \quad (8)$$

where

$$I[e](t) = e(t), \quad \mathcal{I}[e](t) = \int_0^t e(\tau) d\tau, \quad \mathcal{D}[e](t) = \frac{de}{dt}(t).$$

On the other hand, consider the Bessel functions of the first kind  $J_\nu(x)$ , which satisfy the standard differential-recurrence relations (for real  $\nu$ ) [37]

$$J_{\nu-1}(x) + J_{\nu+1}(x) = \frac{2\nu}{x} J_\nu(x), \quad (9)$$

$$2J'_\nu(x) = J_{\nu-1}(x) - J_{\nu+1}(x), \quad (10)$$

where  $'$  denotes differentiation with respect to  $x$ . Equations (9) and (10) can be written in operator form by introducing the differential operator

$$\mathcal{L}_\nu := \frac{d}{dx} - \frac{\nu}{x}, \quad (11)$$

acting on the family  $\{J_\nu\}_{\nu \in \mathbb{R}}$ . Using equations (9) and (10), and definition (11), one writes, respectively,

$$\begin{aligned} J_{\nu+1}(x) &= \left( \frac{\nu}{x} - \frac{d}{dx} \right) J_\nu(x) = -\mathcal{L}_\nu[J_\nu](x), \\ J_{\nu-1}(x) &= \left( \frac{d}{dx} + \frac{\nu}{x} \right) J_\nu(x) = \mathcal{L}_\nu[J_\nu](x). \end{aligned}$$

Analogously to the manner in which a PID controller generates a new control signal  $u$  from the error signal  $e$  via a fixed linear combination of derivative, integral, and identity operators, the Bessel function recurrence relations generate neighboring functions  $J_{\nu\pm 1}$  from  $J_\nu$  through linear combinations of differentiation and multiplication operators.

### A. Analogy Between the Two Structures

Consider  $\mathcal{X}$  as a suitable function space in time (e.g.,  $L^2$  on  $\mathbb{R}_+$ ) and  $\mathcal{Y}$  as a function space in the spatial variable  $x$ . Moreover, consider that the PID operator  $C : \mathcal{X} \rightarrow \mathcal{X}$  is defined by  $C$  given by (8) and the Bessel “shift” operator  $S_\nu : \mathcal{Y} \rightarrow \mathcal{Y}$  can be defined by

$$S_\nu := -\mathcal{L}_\nu \quad (12)$$

acting on the Bessel family via

$$S_\nu[J_\nu](x) = J_{\nu+1}(x). \quad (13)$$

Both  $C$  and  $S_\nu$  are linear operators built by combining primitive operators (differentiation and either integration or multiplication) with scalar coefficients. In particular,  $C$  combines  $I$ ,  $\mathcal{I}$ , and  $\mathcal{D}$  with constants  $K$ ,  $K/T_i$ , and  $KT_d$ , shaping the closed-loop dynamics through proportional, integral, and derivative action. In contrast,  $S_\nu$  combines  $d/dx$  and multiplication by  $\nu/x$  to “shift” the order of the Bessel function while preserving the underlying Bessel differential equation structure.

Formally, one can see both as elements of suitable operator algebras:

$$C \in \text{Alg}\{I, \mathcal{I}, \mathcal{D}\}, \quad S_\nu \in \text{Alg}\left\{\frac{d}{dx}, M_{1/x}\right\}, \quad (14)$$

where  $M_{1/x}$  denotes multiplication by  $1/x$ . The structural analogy is that both control action (via  $C$ ) and order-shifting in Bessel systems (via  $S_\nu$ ) are realized through linear combinations of basic operators that act on a function space and generate families of related signals or modes.

One writes the PID-based increment in the controller variable  $r_\infty$  as [34]

$$\Delta r_\infty(t) = a E(t) + b \frac{dE}{dt}(t) + c \int_0^t E(\tau) d\tau, \quad (15)$$

where  $E(t)$  denotes the error (the difference between the target and measured T inventory), and  $(a, b, c)$  are the proportional, derivative, and integral gains, respectively. Now, one defines the corresponding differential operator as

$$L_{\text{PID}} := b \frac{d}{dt} + a + c\mathcal{I}, \quad (16)$$

where  $\mathcal{I}[E](t) := \int_0^t E(\tau) d\tau$  is the causal integration operator acting on  $E$ . Consider now the classical Bessel operator [37]

$$L_\nu := x^2 \frac{d^2}{dx^2} + x \frac{d}{dx} + (x^2 - \nu^2), \quad (17)$$

acting on sufficiently smooth functions of  $x > 0$ , where  $\nu \in \mathbb{R}$  is a fixed order parameter. Let  $x_0 > 0$  be a reference point and assume that  $x$  is confined to a small neighborhood of  $x_0$ . Then, in this neighborhood,  $L_\nu$  admits the local approximation

$$L_\nu \approx x_0^2 \frac{d^2}{dx^2} + x_0 \frac{d}{dx} + (x_0^2 - \nu^2), \quad (18)$$

which is a second-order linear differential operator with constant coefficients. Furthermore, one writes  $x = \alpha t$  with  $\alpha > 0$  and defines  $y(x) := E(t)$  with  $t = x/\alpha$ . Under this change of variables, equation (18) becomes, up to an overall scaling factor,

$$\tilde{L}_\nu \propto \tilde{a}_2 \frac{d^2}{dt^2} + \tilde{a}_1 \frac{d}{dt} + \tilde{a}_0, \quad \tilde{a}_2 \propto x_0^2, \tilde{a}_1 \propto x_0, \tilde{a}_0 \propto x_0^2 - \nu^2. \quad (19)$$

One can choose  $(a, b, c)$  and the scaling  $\alpha$  such that the first-order representation of the PID operator (15) (viewed at the level of its underlying second-order error dynamics) coincides, up to scaling, with the localized Bessel-type operator  $\tilde{L}_\nu$ . In this sense, the PID increment can be embedded as a special case of a Bessel-type operator acting on the error trajectory  $E(t)$ .

It is important to emphasize that the foregoing identification is not intended to establish a strict global equivalence between the complete Bessel–Sturm–Liouville operator and the discrete PID controller [33, 34]; their spectral formalisms remain distinct. Instead, it demonstrates that after localization around a reference point  $x_0$  (freezing the coefficients at  $x_0$ ) and a suitable rescaling  $x = \alpha t$ , the effective operator governing the PID increment (15) can be viewed as an element of a Bessel-type family, with the controller gains  $(a, b, c)$  playing the role of effective “order” and “scale” parameters associated with  $(\nu, x_0)$ . This provides a formal way to interpret the Li-ratio controller as implementing localized Bessel-type dynamics on the T inventory error.

## B. A Simple Second-Order Error Model

A simple second-order error model can be constructed to match the PID gains  $(a, b, c)$  [34] to the parameters of a localized Bessel operator. The first step is to consider a linearized second-order model for the T inventory error  $E(t)$  of the form

$$E''(t) + a_1 E'(t) + a_0 E(t) = 0, \quad (20)$$

where  $a_0, a_1 > 0$  are the effective sensitivities of the blanket and purification system, respectively, to variations in the control variable. Now, one considers that the PID increment in the controller variable  $r_\infty$  is given by (15). Assuming that the physical system responds approximately proportionally to  $\Delta r_\infty$  on a short time scale, and that the integral term contributes mainly to a slow drift of the operating point, we can associate equation (15), an effective second-order error dynamics of the form (20), with ( $b \neq 0$ )

$$a_1 = \frac{a}{b}, \quad a_0 = \frac{c}{b}. \quad (21)$$

Identifying  $x$  with time  $t$  (or, more generally, taking  $x = \gamma t$  and absorbing  $\gamma$  into a rescaling of coefficients), the associated homogeneous equation for  $E(t)$  is

$$E''(t) + \frac{1}{x_0} E'(t) + \left(1 - \frac{\nu^2}{x_0^2}\right) E(t) = 0. \quad (22)$$

Comparing (22) with the generic form (20), and considering identification (21), we can match PID gains to Bessel parameters, yielding the explicit correspondence ( $a \neq 0, b \neq 0$ )

$$x_0 = \frac{b}{a}, \quad \nu^2 = \left(1 - \frac{c}{b}\right) \frac{b^2}{a^2}. \quad (23)$$

If  $1 - c/b \geq 0$ , then  $\nu$  is real; otherwise,  $\nu$  becomes complex, and the corresponding Bessel-type mode is exponentially modulated. In this way, for any choice of PID gains ( $a, b, c$ ) satisfying the conditions above, the effective second-order error dynamics can be viewed as the localization of a Bessel-type mode of order  $\nu$  around the effective ‘‘radius’’  $x_0 = b/a$ . This provides an explicit parameter map  $(a, b, c) \mapsto (x_0, \nu)$ , realizing the PID controller as a special (localized) case of a Bessel-type operator acting on the error trajectory  $E(t)$ .

To illustrate the mapping (23), consider a simple, dimensionless example in which the PID gains ( $a, b, c$ ) are chosen to be of the same order as typical values used in Ref. [34] (i.e.,  $a$  and  $b$  of comparable size, and  $c$  somewhat smaller, reflecting a less aggressive integral action). Then, for illustration, one assumes

$$a = 0.5, \quad b = 1.0, \quad c = 0.2, \quad (24)$$

and using the explicit relations (23), one obtains the corresponding localized Bessel parameters

$$x_0 = \frac{1.0}{0.5} = 2.0 \text{ and } \nu = \sqrt{3.2} \approx 1.78885. \quad (25)$$

Equivalently, this specific PID tuning may be interpreted as the selection of an effective Bessel-type mode of order  $\nu \simeq 1.8$ , spatially localized in the vicinity of the radius  $x_0 \simeq 2$ . We reiterate

that this identification is intrinsically local in nature: the PID operator is derived as a second-order, constant-coefficient approximation of a Bessel-type Sturm–Liouville operator in the neighborhood of a chosen reference point, rather than being established through a global spectral equivalence.

During the time interval  $t \in [t_1, t_2]$ , the Bessel mode of order  $\nu$  exhibits error dynamics that are accurately approximated by a second-order model parameterized by the coefficients  $(a_0, a_1)$ , which, in turn, correspond to a set of effective PID gains  $(a, b, c)$ . Within this regime, the resulting closed-loop T-dynamics are, to leading order, indistinguishable from those generated by a conventional PID controller.

## V. TRITIUM BREEDING RATIO

The TBR (Tritium Breeding Ratio) is suitable for connecting the neutronic behavior of Li-based blankets with the PID-Bessel framework developed above. One assumes that

$$n_6(t) + n_7(t) = n_{Li,tot} \quad (26)$$

where  $n_6(t)$  and  $n_7(t)$  are, respectively, the number density of  ${}^6\text{Li}$  and  ${}^7\text{Li}$  in the breeder region at time  $t$ . Furthermore,  $n_{Li,tot}$  is the total lithium density (or inventory) at time  $t$ , assumed to be constant. The fraction of total lithium that is  ${}^6\text{Li}$  at time  $t$  is given by the enrichment ratio of  ${}^6\text{Li}$ , written as

$$R(t) = \frac{n_6(t)}{n_6(t) + n_7(t)} \in [0, 1], \quad (27)$$

and the error  $E(t)$  is assumed to be proportional to  $\text{TBR}(t) - \text{TBR}_{target}$ .

It is important to stress that in detailed MCNP/FISPACT calculations, TBR is a non-linear function of density, geometry, and neutron spectrum [25, 34]. However, based on the operating regime relevant for feedback control, the dependence of TBR and impurity levels on the chosen control parameters (such as  ${}^6\text{Li} : {}^7\text{Li}$  enrichment) is empirically close to linear, which motivates the use of linear controllers and local first-order (Taylor) approximations around a design point [24, 33]. Therefore, one writes

$$\text{TBR}(t) \approx \alpha R(t) + \beta, \quad (28)$$

where  $\alpha$  is the sensitivity of TBR to changes in the  ${}^6\text{Li}$  enrichment near the operating point, whereas  $\beta$  is the offset of the linear approximation.

In this simple model, one evolves the control variable  $R(t)$  while preserving (26). One also defines  $E(t)$  from the linear TBR( $t$ ) given by the approximate relation (28) into  $R(t)$ . Applying the second-order Bessel equation and keeping Li:Pb = 17:83 and  ${}^6\text{Li} + {}^7\text{Li}$  constant.

Figure 4 shows a representative time trace of the  ${}^6\text{Li}$  enrichment  $R(t)$  and the corresponding TBR( $t$ ) computed from the linear surrogate model, illustrating that the controller operates in a regime of small, bounded deviations around  $\text{TBR} \simeq 1$ . Considering different values for  $\nu$ , we adopt  $\alpha = 0.08$  and  $\beta = 1.0$  in the linear surrogate equation (28), so that the system operates in a regime of small, bounded deviations  $0.90 \lesssim \text{TBR}(t) \lesssim 1.10$  [11–13, 26, 27] around the self-sufficiency point. It is important to stress that for each  $\nu$ , the corresponding dashed line lies almost on top of the solid one in the chosen time window, which means the closed-loop error dynamics are well approximated by a second-order LTI model for all those Bessel orders. Changing  $\nu$  shifts the phase and waveform of  $E''(t)$ , but their amplitude and frequency remain similar, consistent with small, bounded deviations of TBR around the target. Therefore, different “localized Bessel modes” (different  $\nu$ ) still correspond to low-order, PID-like dynamics for the tritium inventory error.

Notice that the  $\alpha$  and  $\beta$  coefficients are effective local fit parameters that approximate how TBR responds to changes in the  ${}^6\text{Li}$  enrichment ratio  $R(t)$  near a chosen design point, as obtained by linearizing higher-fidelity neutronics calculations such as DEMO blanket studies. Thus,  $\alpha$  and  $\beta$  are not global sensitivities of a specific blanket concept, but convenient reduced parameters for studying feedback control within a physically motivated operating window.

## VI. JET THERMAL AND PID-BESSEL CONTROLLER

To validate the theoretical framework developed in the preceding sections, we conducted a numerical experiment in Python that integrates a reduced jet/blanket model with the previously described PID–Bessel computational framework. The jet thermal response is modeled using a lumped-parameter temperature field  $T(t)$ , which obeys a first-order relaxation equation derived by analogy with the coupled mass and heat transport system (3)–(6). The evolution of  $T(t)$  is driven by a Bessel-modulated heat source  $q_{\text{in}}(t)$ , constructed to emulate the spatially and temporally structured energy deposition associated with energetic deuteron beams. A PID controller, expressed in the operator formulation of equation (7) and definition (8), operates on the control error  $E(t) = T_{\text{target}} - T(t)$ .

The resulting closed-loop error response is subsequently approximated by a second-order model, whose coefficients are then mapped onto effective Bessel parameters using the previously derived

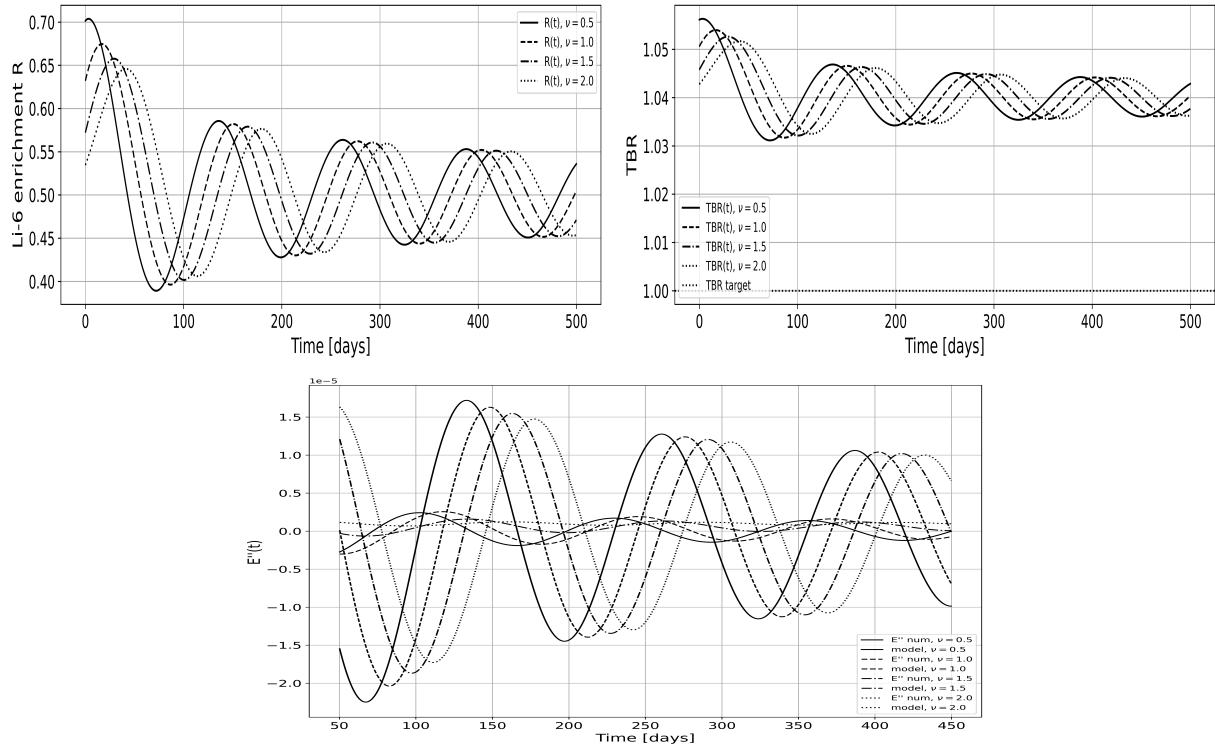


Figure 4. Time evolution of the  ${}^6\text{Li}$  enrichment ratio  $R(t)$  (top left) and the corresponding tritium breeding ratio  $TBR(t)$  (top right) obtained from the linear surrogate model (28), together with the target  $TBR_{\text{target}} = 1.0$ . The bottom panel shows the second derivative of the tritium-inventory error  $E''(t)$  (solid curves) and the corresponding least-squares second-order fits  $E''(t) + a_1 E'(t) + a_0 E(t) \simeq 0$  (dashed curves) for several Bessel orders  $\nu$ . For all cases, the controller maintains small, bounded deviations  $0.90 \lesssim TBR(t) \lesssim 1.10$ , and the error dynamics are well described by a low-order LTI model.

relations. This procedure explicitly demonstrates that a physically motivated Li-based system, such as the IFMIF-DONES liquid-Li jet or a fusion blanket surrogate, can exhibit local error dynamics that are accurately characterized by a Bessel-type operator using PID control.

Figure 5, left panel, shows the numerically computed second derivative of the tritium inventory error  $E(t)$  (solid lines) together with the least squares second-order approximation  $E''(t) + a_1 E'(t) + a_0 E(t) \simeq 0$  (dashed lines) for several values of  $\nu$ . The close overlap between numerical and fitted curves indicates that, over the chosen time window, the closed-loop error dynamics are well described by a low-order linear model compatible with the localized Bessel-type operator. The right panel shows the corresponding jet temperature trajectories  $T(t)$  for different Bessel-modulated heat-source orders  $\nu$ . It demonstrates that, despite the differing transient oscillations, the PID controller robustly drives the system toward the same thermal operating point near  $T_{\text{target}}$ , confirming that a range of effective Bessel-type source modulations remains compatible with stable, well-controlled

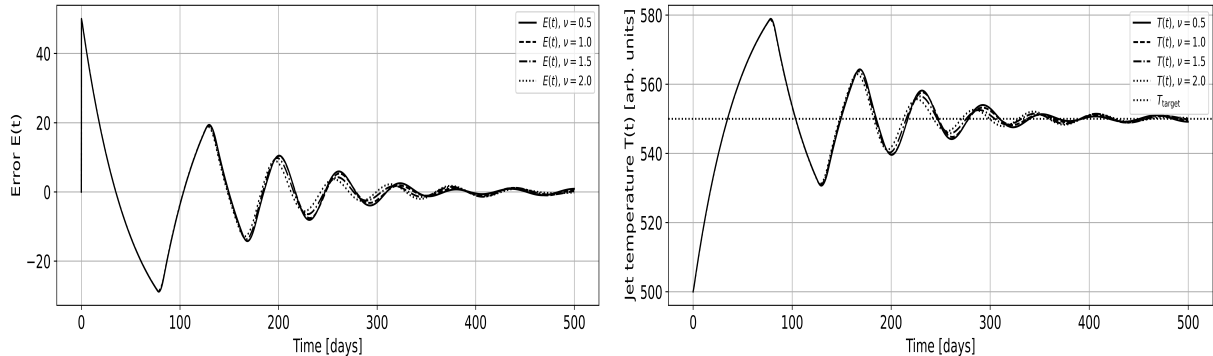


Figure 5. Numerically computed second derivative of the tritium-inventory error  $E(t)$  (left panel) from the reduced jet/blanket-PID model (solid curves) and corresponding least-squares fits to the second-order approximation  $E''(t) + a_1 E'(t) + a_0 E(t) \simeq 0$  (dashed curves) over the approximately linear time window. The close agreement indicates that the closed-loop error dynamics are well captured by a low-order model compatible with the localized Bessel-type operator. The right panel shows that, for different  $\nu$  (Bessel orders), the closed-loop jet temperature always relaxes smoothly to the same target value with only mild oscillations.

jet temperatures.

## VII. DISCUSSION AND FINAL REMARKS

Lithium-based components in D-T fusion systems both breed tritium and remove heat in tokamak blankets and deuterium-lithium neutron sources. We combine nuclear data for D-T and lithium reactions, simplified thermohydraulic modeling of a liquid Li jet, and an operator-theoretic feedback-control description to reveal the coupling between neutronics, thermal management, and control in these systems.

The jet thermal-expansion model, based on mass conservation and heat conduction, demonstrates that pronounced beam loading induces temperature and velocity perturbations that can be quantitatively characterized by a small set of scalar observables, such as the peak temperature and the maximum transverse velocity. These observables are natural error variables for feedback design and support low-order dynamical models, as in our lumped jet-temperature example driven by a Bessel-modulated heat source.

Writing the continuous-time PID law as a linear operator and comparing it with Bessel differential recurrences exposes a structural analogy. Localizing the Bessel operator around a reference

point and introducing a simple second-order error model yields an explicit mapping between PID gains  $(a, b, c)$  and effective Bessel parameters  $(x_0, \nu)$ . Thus, the PID increment can be seen as a localized Bessel-type operator on the tritium-inventory error. This identification is local but still allows interpreting specific PID tunings as selecting effective Bessel modes near an operating point.

In contrast to prior studies that primarily addressed numerical PID tuning for tritium breeding regulation, this work provides an analytical formulation in which the PID gains are embedded within a Bessel-type operator, thereby elucidating the modal structure of low-order Li-based feedback systems.

Several limitations of this work suggest natural directions for future research. First, the thermohydraulic and TBR models are intentionally simplified and cannot replace full 3D Monte Carlo and CFD simulations; the PID–Bessel correspondence should be tested with higher-fidelity models and more realistic operating scenarios. Second, because our construction relies on linearization and local approximation, the mapping is expected to hold only near a chosen operating point; extending the analysis to explicitly nonlinear controllers or gain-scheduled strategies could broaden its validity. Third, we have considered only scalar error variables. In contrast, practical systems involve multiple coupled control loops (e.g., tritium inventory, outlet temperature, impurity concentration), motivating a multivariable generalization of the Bessel-type operator framework.

Despite these limitations, our results offer an initial step toward a unified treatment of tritium breeding, thermal management, and feedback control in Li-based fusion technologies. By linking D-T reaction physics, Li-breeding chemistry, jet thermohydraulics, and PID-Bessel operator theory, this work provides a conceptual framework to guide future numerical studies with detailed neutronics and CFD, as well as experiments in facilities such as IFMIF-DONES and next-generation tokamak blankets.

## ACKNOWLEDGMENTS

The acknowledgments are extended to UFSCar by SASB and SDC for their contributions.

- 
- [1] International Atomic Energy Agency Bulletin. Fusion Energy. <https://www.iaea.org/sites/default/files/fusionenergy.pdf>
  - [2] A. Ciampichetti, P. Rocco, and M. Zucchetti. Accidental and Long-Term Safety Assessment of Fission and Fusion Power Reactors. *Fusion Engineering and Design* 63-64, 229-234 (2002).

- [3] W. M. Nevins. A Review of Confinement Requirements for Advanced Fuels. *Journal of Fusion Energy* 17(1), (1998).
- [4] MIT MITEI. The Role of Fusion Energy in a Decarbonized Electricity System, (2024): [https://energy.mit.edu/wp-content/uploads/2024/09/MITEI\\_FusionReport\\_091124\\_final\\_COMPLETE-REPORT\\_fordistribution.pdf](https://energy.mit.edu/wp-content/uploads/2024/09/MITEI_FusionReport_091124_final_COMPLETE-REPORT_fordistribution.pdf)
- [5] J. Hu *et al.*. All Superconducting Tokamak: EAST. *AAPPS Bulletin* 33, 8 (2023): <https://doi.org/10.1007/s43673-023-00080-9>
- [6] S. Ding *et al.*. A High-Density and High-Confinement Tokamak Plasma Regime for Fusion Energy. *Nature* 629, 555-560 (2024).
- [7] R. Villari *et al.*. Overview of Deuterium-Tritium Nuclear Operations at JET. *Fusion Engineering and Design* 217, 115113 (2025).
- [8] E. R. Solano. Fusion Research in a Deuterium–Tritium Tokamak. *Fund. Plasma Phys.* 15, 100096 (2025).
- [9] H.-S. Bosch and G. M. Hale. Improved Formulas for Fusion Cross-Sections and Thermal Reactivities. *Nucl. Fusion* 32(4), 611 (1992).
- [10] R. S. de Souza *et al.*. Thermonuclear Fusion Rates for Tritium Deuterium Using Bayesian Methods. *arXiv:1901.04857* (2019).
- [11] M. E. Sawan and M. A. Abdou. Physics and Technology Conditions for Attaining Tritium Self-Sufficiency for the DT Fuel Cycle. *Fusion Engineering and Design* 81, 1131–1144 (2006).
- [12] L. A. El-Guebaly and S. Malang. Toward the Ultimate Goal of Tritium Self-Sufficiency: Technical Issues and Requirements Imposed on ARIES Advanced Power Plants. *Fusion Engineering and Design* 84, 2072–2083 (2009).
- [13] M. Abdou *et al.*. Physics and Technology Considerations for the Deuterium–Tritium Fuel Cycle and Conditions for Tritium Fuel Self Sufficiency. *Nucl. Fusion* 61, 013001 (2021).
- [14] J. D. Lee. Tritium Breeding and Direct Energy Conversion. *Proc. of the Am. Chem. Soc. Symposium on The Role of Chemistry in the Development of Controlled Fusion*. Boston, Massachusetts, (1972): [https://inis.iaea.org/records/ehtrj-62m95/preview/4037886.pdf?include\\_deleted=0](https://inis.iaea.org/records/ehtrj-62m95/preview/4037886.pdf?include_deleted=0)
- [15] P. Mánek *et al.*. Fast Regression of the Tritium Breeding Ratio in Fusion Reactors. *Mach. Learn.: Sci. Technol.* 4, 015008 (2023).
- [16] L. Morgan and J. Pasley. Tritium Breeding Control Within Liquid Metal Blankets. *Fusion Engineering and Design* 88, 107–112 (2013).
- [17] T. Flament, P. Tortorelli, V. Coen, and H. U. Borgstedt. Compatibility of Materials in Fusion First Wall and Blanket Structures Cooled by Liquid Metals. *Journal of Nuclear Materials* 191-194, 132-138 (1992).
- [18] S. Fukada, Y. Edao, and A. Sagara. Effects of Simultaneous Transfer of Heat and Tritium Through Li–Pb or Flibe Blanket. *Fusion Engineering and Design* 85, 1314–1319 (2010).

- [19] A. Loarte *et al.*. Initial Evaluations in Support of the New ITER Baseline and Research Plan. Report no. ITR-24-004, (2024): <https://www.iter.org/sites/default/files/media/2024-04/itr-24-004-baseline-ok.pdf>
- [20] R. A. Pitts *et al.*. Plasma-Wall Interaction Impact of the ITER Re-Baseline. *Nuclear Materials and Energy* 42, 101854 (2025): <https://www.sciencedirect.com/science/article/pii/S2352179124002771?via%3Dihub>
- [21] J. Aubert *et al.*. Status of the EU DEMO HCLL Breeding Blanket Design Development. *Fusion Engineering and Design* 136(B), 1428-1432 (2018).
- [22] F. A. Hernandez *et al.*. Overview of the HCPB Research Activities in EUROfusion. *IEEE Transactions on Plasma Science* 46(6), 2247-2261 (2018).
- [23] G. Zhou, Y. Lu, and F. A. Hernández. A Water Cooled Lead Ceramic Breeder Blanket for European DEMO. *Fusion Engineering and Design* 168, 112397 (2021).
- [24] L. Morgan and J. Pasley. The Impact of Time Dependant Spectra on Fusion Blanket Burn-up. *Fusion Engineering and Design* 88, 100-105 (2013).
- [25] D.W. S. Clark *et al.*. Breeder Blanket and Tritium Fuel Cycle Feasibility of the Infinity Two Fusion Pilot Plant. *J. Plasma Phys.* 91, E86 (2025).
- [26] W. Kuan and M. A. Abdou. A New Approach for Assessing the Required Tritium Breeding Ratio and Startup Inventory in Future Fusion Reactors. *Fusion Technology* 35, 309 (1999).
- [27] S. Zheng T. N. Todd. Study of Impacts on Tritium Breeding Ratio of a Fusion DEMO Reactor. *Fusion Engineering and Design* 98–99, 1915-1918 (2015).
- [28] M. Abdou *et al.*. Physics and Technology Considerations for the Breeding Blanket. *Nucl. Fusion* 61(1), 013001 (2021).
- [29] J. Knaster *et al.*. IFMIF, the European–Japanese Efforts Under the Broader Approach Agreement Towards a Li(d,xn) Neutron Source: Current Status and Future Options. *Nuclear Materials and Energy* 9, 46-54 (2016).
- [30] G. D’Ovidio, F. Martín-Fuertes, J. C. Marugan, S. Bermejo, and F. S. Nitti. Lithium Fire Protection Design Approach in IFMIF-DONES Facility. *Fusion Engineering and Design* 189, 113446 (2023).
- [31] A. Hassanein. Deuteron Beam Interaction with Lithium Jet in a Neutron Source Test Facility. *Journal of Nuclear Materials* 233-237, 1547-1551 (1996).
- [32] A. Möslang. IFMIF: the Intense Neutron Source to Qualify Materials for Fusion Reactors. *C. R. Physique* 9, 457–468 (2008).
- [33] K. J. Åström and R. M. Murray. *Feedback Systems: An Introduction for Scientists and Engineers*, 2nd. edition, (2020).
- [34] L. Morgan and J. Pasley. Tritium Breeding Control within Liquid Metal Blankets. *Fusion Engineering and Design* 88, 107-112 (2013).
- [35] H. Wang *et al.*. Enhancement of Element Production by Incomplete Fusion Reaction with Weakly Bound Deuteron. *Commun. Phys.* **2**, 78 (2019).

- [36] B. Wielunska, M. Mayer, T. Schwarz-Selinger, U. von Toussaint, and J. Bauer. Cross Section Data for the  $D(^3\text{He}, p)^4\text{He}$  Nuclear Reaction from 0.25 to 6 MeV. Nucl. Instrum. and Meth. in Phys. Research B 371, 41 (2016).
- [37] G. B. Arfken and H. J. Weber. Mathematical Methods for Physicists, 6th edition. Harcourt, (2005).
- [38] Y. Jianga, S. Adulojua, and S. Smolentsev. Design and Analysis of the Open-Surface Slow Li Flow Divertor and Comparison to Fast Li Flow Divertor. Fusion Science and Technology 82(1–2), 135–155 (2026).